Journal of Thermal Science Vol.24, No.3 (2015) 246–253

DOI: 10.1007/s11630-015-0780-4 **Article ID: 1003-2169(2015)03-0246-08**

Numerical Simulation of Flow Characteristics in Micro Shock Tubes

Guang Zhang[1], Toshiaki Setoguchi[2] and Heuy Dong Kim[1*]

1. Department of Mechanical Engineering, Andong National University, Andong, 760-749, Korea
2. Department of Mechanical Engineering, Saga University, Saga, Japan

Recently micro shock tubes have been widely used in many engineering and industrial fields, but the characteristics of unsteady flow are not well known to date in micro shock tubes. Compared to conventional shock tubes with macro scales, flows related to shock waves in micro shock tubes are highly complicated. Stronger viscous and dissipative interactions make shock wave dynamic behaviors significantly different from theoretical predictions. In the present study, a CFD work was applied to the unsteady compressible Navier-Stokes equations which were solved using a fully implicit finite volume scheme. The diaphragm pressure ratio and shock tube diameter were varied to investigate their effects on micro shock tube flows. Different wall boundary conditions were also performed to observe shock wave and contact surface propagation with no slip and slip walls. Detailed flow characteristics at the foot of shock wave and contact surface propagation were known from the present numerical simulations.

Keywords: Micro shock tube, Shock wave propagation, Slip wall, Unsteady flow, CFD

Introduction

In the past decades, micro shock tubes have been widely used in various engineering applications, such as micro turbines, micro combustions, and needle-free delivery devices. Micro shock tubes consist of the driver section and driven section which are separated by a diaphragm. After the diaphragm is ruptured due to the pressure difference between driver section and driven section, the shock wave happens and the flow behind the shock wave is induced to move by the shock wave propagation. The shock wave and contact surface move towards the driven section and the expansion wave moves into the driver section. Shock flows demand further consideration of dissipative effects which are usually absent in macro shock tube flows.

Due to the low pressure and micro scale in micro shock tube, viscous and rarefaction effects are much more prominent. This makes simulated and experimental results of the shock wave propagation and flow characteristics more deviation from theoretical analysis. Compared to the traditional shock tubes, the thicker boundary layer leads to more attenuation in shock wave and flow motion in micro shock tube, but the contact surface is accelerated due to the boundary layer formation. Heat conduction phenomena commonly ignored in conventional shock tubes, play an important role in the micro shock tubes, and viscous stresses attenuate both velocity of the flow and shock wave propagation, which makes experimental study difficult to perform compared to numerical analysis. Even though micro shock tubes have investigated for a long time, there are still some unexplored and unexplained effects on shock wave attenuation to date.

Received: November 2014 Kim, H.D.: Professor
This work was supported by the National Research Foundation of Korea (NRF) grant funded by the Korea government (MEST) (2011-0017506).

Nomenclature

P	Static pressure (atm)	γ	Specific heat ratio
Pr	Pressure ratio	ρ	Density (kg/m^3)
T	Total temperature (K)	δ	Boundary layer thickness (mm)
a	Speed of sound (m/s)	λ	Molecular mean free path
L	Distance between shock wave and contact surface (mm)	σ	L-J characteristics length of gas molecules
M	Mach number	**Subscripts**	
u	Velocity (m/s)	1	Driven section
t	Time (ms)	4	Driver section
x	Axial coordinate	w	wall
μ	Dynamic viscosity (Pa·s)	g	gas
D	Shock tube diameter (mm)	c	cell center

Duff R. E.[1] studied the viscous loss associated with the boundary layer growth in shock wave propagation in his experimental study. An electron beam densitometer was used for observing shock velocity attenuation at low pressures in shock tubes. The initial pressure ratio was also observed to influence the shock strength. Brouillette M.[2] investigated unsteady micro scale compressible flows experimentally. He introduced a control volume model and proposed a scaling parameter S that indicates effects of the scale. Diffusive effects of the friction and heat conduction were studied at low S values in micro shock tubes. Results showed that the model predicted the shock wave at small scale to experience much loss in strength. In addition, experimental results had quantitative agreement with the theoretical conclusion from the proposed model at low driven pressures in micro shock tubes.

Mirels H.[3] introduced an analytical method to evaluate boundary layer influence on shock wave propagation. It was assumed that the shock wave moves with uniform velocity, and the flow was investigated in a shock fixed coordinate system. Sturtevant B.[4] and Kohsuke Tanaki[5] et al investigated the influence of boundary layer on the shock wave propagation at different boundary conditions. Good agreement was observed between simulations and theoretical results for the laminar portion of the boundary layer. Ngomo D.[6] studied the wall friction and heat transfer effects on the shock wave propagation in a micro shock tube. They found that diffusive shear stresses and energy losses near the wall significantly led to shock wave attenuation.

Sun M.[7] et al performed numerical and experimental studies on shock wave propagation in narrow channels with height ranging from 1mm to 16mm. The channel flow was visualized by using "double exposure holographic interferometry" technique, and pressure transducers were used for recording pressure changes at different locations. Experimental results had a good agreement with numerical results. Xiao Hu[8] et al conducted an experimental study on the shock wave attenuation compared to the theoretical results. The decrease in shock wave velocity was performed at different low Reynolds numbers. Results showed that the viscosity of the flow dominated the shock wave attenuation as the shock wave propagated in the overlong channel. Bhasakaran K. A.[9] used chemical kinetics and high temperature gas flow to study flows in shock tubes.

Zeitoun D. E. et al[10-11] studied the application of unsteady Navier-Stokes equations coupled with the velocity slip and temperature jump boundary conditions to micro shock tube flows. A strong decrease in the shock strength and the flow velocity along the micro shock tube was observed by them. The decay of shock wave strength was much stronger at lower initial pressure and small tube diameter. Based on the Knudsen number, which indicates the rarefaction effect, Arun K.R. et al[12-13] performed computational studies to investigate the shock wave propagation under different pressure ratios, shock tube diameters with slip condition and no slip wall boundary conditions. The results indicated shock wave propagation is attenuated by viscous boundary layer formation, and the decay of the shock wave increase drastically with reduction in diameter. Park J. O et al[14] performed an experimental study to investigate shock wave propagation and shock wave attenuation. Results indicated shock wave attenuation happened much more in the micro shock tube of smaller scale.

This paper mainly focuses on observing shock wave, contact surface propagation and on giving an indepth analysis for shock wave attenuation at different conditions. In the present study, numerical investigations were carried out in micro shock tube models. Effects of different diaphragm pressure ratios were investigated for constant atmosphere pressure in the driver section. Effects of the shock tube diameter on shock wave and contact surface propagation were also investigated. Different wall boundary conditions of no slip and slip walls were used to observe unsteady flow characteristics. The scal-

ing parameter S indicating effects of the scale were calculated.

Theoretical analysis

Shock tube theory

Shock wave and contact surface are induced by the ruptured diaphragm. The shock wave and contact surface move towards the driven section with Mach number M_S and M_C. In an ideal shock tube at fixed initial conditions both in driver and driven sections, M_S and M_C can be calculated as:

$$\frac{P_4}{P_1}=\left\{1+\frac{2\gamma_1}{\gamma_1+1}\left(M_S^2-1\right)\right\}\cdot \left\{1-\frac{\gamma_4-1}{\gamma_4+1}\frac{\alpha_1}{\alpha_4}\left(M_S-\frac{1}{M_S}\right)\right\}^{-2\gamma_4/\gamma_4-1} \tag{1}$$

$$M_C=\frac{1}{\gamma_1}\left(\frac{P_2}{P_1}-1\right)\sqrt{\frac{\frac{2\gamma_1}{\gamma_1+1}}{\frac{P_2}{P_1}+\frac{\gamma_1-1}{\gamma_1+1}}}\sqrt{\frac{1+\frac{\gamma_1+1}{\gamma_1-1}\frac{P_2}{P_1}}{\frac{\gamma_1+1}{\gamma_1-1}\frac{P_2}{P_1}+\left(\frac{P_2}{P_1}\right)^2}} \tag{2}$$

Shock wave Mach number and contact surface Mach number keep constant in micro shock tube as all boundary conditions are fixed. M_S and M_C increase with the increase of the diaphragm pressure ratio. However, due to the attenuation happens in the real shock tube flow resulting from viscous and rarefaction effects, shock wave and contact surface Mach number always show difference from the theoretical solutions. Shock wave Mach number gradually decreases, but contact surface Mach number gradually increases. The formation and development of the boundary layer behind the shock wave is the main reason for this.

Scaling parameter S

Diffusive transport phenomena, such as the heat conduction and shear stresses, make remarkable deviation in flow characteristics compared to ideal shock wave behaviors in a micro shock tube as demonstrated by Brouillette[2]. A control volume obtaining from the region between the shock wave and contact surface was proposed to quantify effects of the scale and diffusive transport phenomena on shock wave propagation as is shown in Fig. 1. SW, CS and EH respectively represent shock wave, contact surface and expansion head. The friction and heat transfer to side walls are described by appropriate source terms through this control volume approach. As the shock wave and contact surface propagate in the driven section, the length of control volume becomes larger due to velocity difference between the shock velocity and contact surface velocity. Based on the control volume, the scaling parameter S indicating effects of the scale was used in Eq. (3).

$$\frac{P_2}{P_1}=\frac{\rho_2}{\rho_1}\left\{1+\frac{\gamma_1-1}{2}M_S^2\left[1-\left(\frac{\rho_1}{\rho_2}\right)^2\right]\right\} -\frac{\rho_2}{\rho_1}\left(\frac{4L}{D\,\mathrm{Re}}\right)\frac{1}{M_S\,\mathrm{Pr}}\left[\frac{P_2}{P_1}\frac{\rho_1}{\rho_2}-1\right] \tag{3}$$

$$S=\frac{\mathrm{Re}*D}{4L} \tag{4}$$

Reynolds number and the distance L are two important variable to calculate S. It should be noted that Re= $u_2\rho_2D/\mu_2$. The velocity, density and dynamic viscosity of the flow are obtained from the region between the shock wave and contact surface. Indeed, effects of the scale are investigated by calculating Reynolds number and the distance L of the control volume. Effects of the scale enhance with the increase of Reynolds number and the decrease of the distance L. Eq. (3) indicates that a smaller S value will have more obvious effects on calculating density ratio between the front and back of the shock wave. Lower Reynolds number and larger distance L will contribute to smaller S values. If S becomes infinite, effects of the scale can be ignored. This happens in shock tubes with large diameters and high Reynolds numbers.

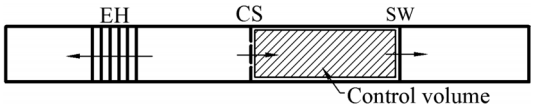

Fig. 1 Control volume used in the study of diffusive effects in the micro shock tube

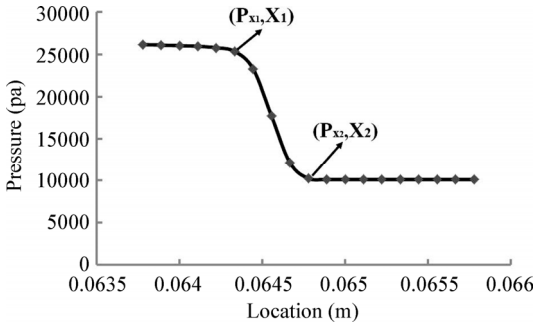

Fig. 2 Partial pressure distributions along the axis at t=0.12 ms (D=3 mm, Pr=10)

Pressure gradient

As the shock wave moves in micro shock tube, the pressure gradient of the flow in front of and after the shock wave changes. The pressure gradient is related to the pressure difference in front of and after the shock wave and the distance across shock wave as is shown in Fig. 2. The pressure gradient can be calculated by the

following Eq. (5).

$$\frac{\partial P}{\partial X}=\left|\frac{P_{X_2}-P_{X_1}}{X_2-X_1}\right| \tag{5}$$

Non-dimensional pressure gradient can be expressed as:

$$C=\frac{\partial P}{\partial X}*\frac{D}{P_1}=\left|\frac{P_{X_2}-P_{X_1}}{X_2-X_1}\right|*\frac{D}{P_1} \tag{6}$$

Where $|P_{X2} - P_{X1}|$ represents the pressure difference across the shock wave. $|X_2 - X_1|$ is the distance of pressure change across the shock wave.

Slip wall boundary conditions

The slip wall boundary condition was performed at low pressure by using Maxwell's slip velocity and temperature jump equations, as is shown below[15].

$$U_w-U_g=\frac{\lambda}{\delta}\left(\frac{2-a_v}{a_v}\right)\left(U_g-U_c\right) \tag{7}$$

$$T_s-T_w=2\frac{\lambda}{\delta}\left(\frac{2-a_T}{a_T}\right)\left(T_g-T_c\right) \tag{8}$$

$$\lambda=\frac{k_BT}{\sqrt{2}\pi p\sigma^2} \tag{9}$$

Where a_v and a_T are the momentum and thermal accommodation coefficients respectively. User defined functions were written to indicate the wall shear stress responsible for the slip velocity jump by Eq. (7) and temperature jump by Eq. (8).

Computational study

Computational domain

Unsteady flows were simulated with the driver section and driven section filled in with ideal gas at different initial conditions in micro shock tube models. For the present study, a 2D axisymmetric micro shock tube model was numerically simulated as is shown in Fig. 3. All sections are circular in cross-section with same diameter. The driver section is 100mm long and the driven section has a length of 200 mm. Five points are mounted at the axis of the simulated shock tube model to record the pressure changes.

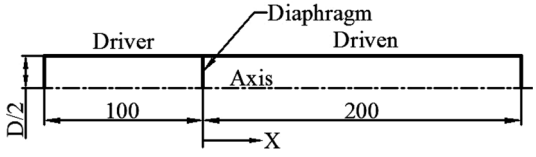

Fig. 3 Schematic of computational domain

Numerical schemes

Fine structured quad grids were created with boundary layers near walls in all simulation regions. Fine boundary layer grids were required to exactly investigate boundary layer effects on shock wave attenuation. The driver section and driven section were filled with air assumed as ideal gas. The flow properties were mathematically analyzed by solving unsteady Reynolds Averaged Navier-Stokes equations. SST *k*-ω model was chosen for the turbulence model and Sutherland viscosity model showing variable viscosity with temperature change was used as viscosity model. AUSM scheme was used as the flux model and the second order implicit scheme was used for temporal discretization. Spatial discretization was described by using second order upwind scheme. The driver and driven sections were patched with their corresponding initial pressures.

Boundary conditions

Effects of the diaphragm pressure ratio and shock tube diameter were studied at different initial pressures in driven section and shock tube diameters. Different wall boundary conditions were also performed. Both sections were initialized with the constant total temperature of 300K. The details are given in Table 1 and Table 2.

Commercial solver, Fluent, was used for the simulation of the present micro shock tube models. The mesh size for simulated model was 163,000 and the minimum cell led to the iteration time step size of 10^{-8} s. The driver section was filled with high pressure ideal gas of atmospheric pressure. Different low pressures were specified in the driven section.

The diaphragm boundary condition was wall at the beginning. The wall was instantaneously changed to be interior, which was regarded as that the diaphragm was suddenly ruptured. Before the diaphragm was ruptured, in order to check the initializations and boundary conditions, the simulation was performed in some time. After this, the diaphragm was suddenly ruptured. The tube walls were assumed to be adiabatic walls with a constant temperature of 300K.

Table 1 Detailed parameters for different driven pressure

Cases	P_4/P_1	P_1	$T_{1,4}$(K)	Diameters(mm)
1	10	0.1	300	3
2	20	0.05	300	3
3	100	0.01	300	3

Table 2 Initial conditions for different cases

Cases	P_4/P_1	P_1	Diameters(mm)	Wall conditions
1	10	0.1	3	No slip
4	10	0.1	1	No slip
5	10	0.1	3	Slip

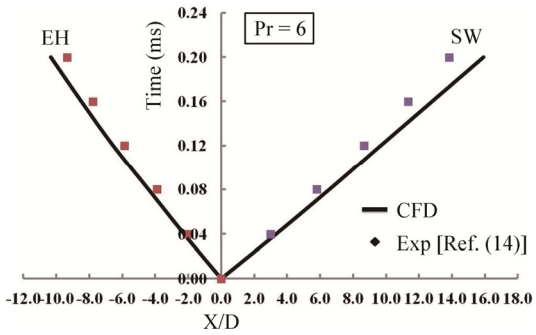

Fig. 4 Comparison between experimental and CFD waves locations at various time. (D=6mm)

Validation

A comparison between experimental results and CFD results was performed to validate the accuracy of present numerical simulations. The experimental data was taken from reference[14] where a micro shock tube model with 6mm diameter was studied at diaphragm pressure ratio of 6. The driver section was initialized at the pressure of 6 atm, and the driven section was kept at atmosphere pressure. Shock wave and expansion wave propagation curves were obtained as is shown in Fig. 4. SW and EH respectively represent shock wave and expansion head. As the expansion head did not touch the tube wall, the wave x-t diagram was obtained. Results show that acceptable deviations were observed except that more attenuation happened in experimental study. This is due to much more viscous effects in real gas. In addition, the heat transfer happened between shock heated gas and tube walls also affected this deviation. Walls are assumed to be adiabatic and kept the constant temperature of 300K in CFD simulation. Therefore, numerical simulations used for the present study can predict flow characteristics in shock tubes.

Results and Discussions

Different initial driven pressures were used to study the shock wave propagation as is shown in Table 1. As expansion waves did not reach the end wall in driver section, pressure histories along the axis were obtained for three cases as is shown in Fig. 5. Shock wave gradually attenuated as it moved in the shock tube, which can be seen from the decrease of shock wave strength. This results from viscous effects, the friction between shock wave front and tube walls and the boundary layer formation behind the shock in micro shock tube. At the same time the location of shock wave is much further at diaphragm pressure ratio of 100 compared to that at diaphragm pressure ratios of 10 and 20. This indicates that as the pressure ratio increases, the shock wave velocity also increases, which has a good agreement with the theoretical results from Eq. (1).

The distributions of pressure gradient of flow in front and after shock wave calculated from Eq. (6) are shown in Fig. 6. As the shock wave moved through the driven section, the pressure gradient gradually decreased. This mainly results from that shock wave strength decreased and the distance of pressure change across shock wave increased. At the beginning, the pressure gradient is relatively high, which is attributed to smaller distance of pressure change across shock wave. After shock wave moved a certain time, the change of pressure gradient becomes small. This change can be regarded as linear change.

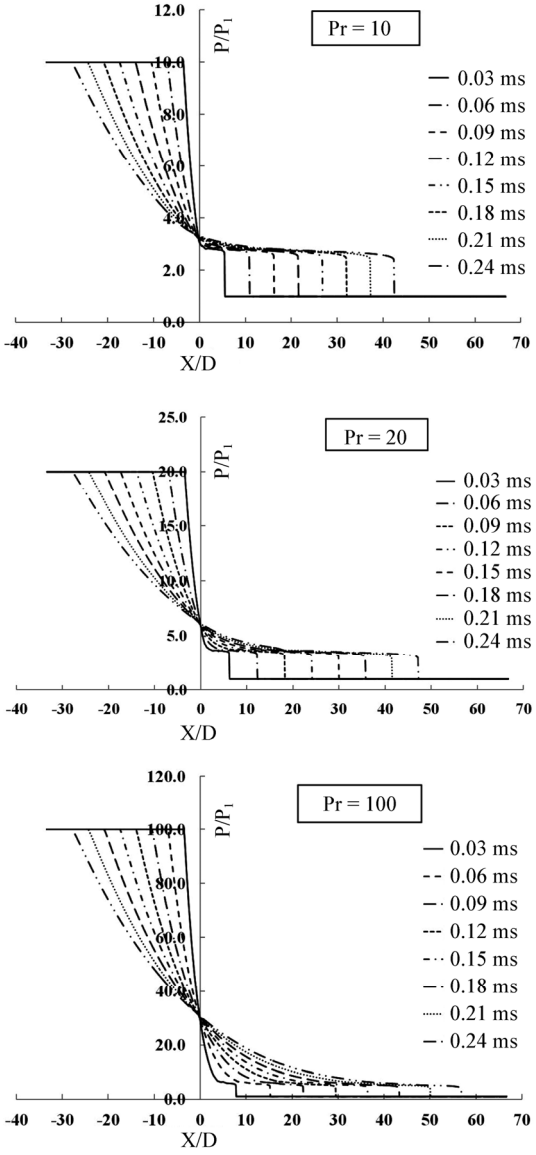

Fig. 5 Pressure histories along axis at different diaphragm pressure ratios (D=3mm)

Reynolds number distributions in the region between shock wave and contact surface were obtained at different diaphragm pressure ratios as is shown in Fig. 7. The density, velocity and dynamic viscosity of the flow

changed as the shock wave and contact surface moved through the driven section. Reynolds number increases at these three cases mainly due to the flow velocity gradually increases in this region. In addition, the flow density also increases. Reynolds number is much less at the pressure ratio of 100 due to the lower density compared to other two cases. The low density is caused by the low driven pressure at the high pressure ratio in the micro shock tube.

The distributions of scaling parameter S values calculated by Eq. (4) at different diaphragm pressure ratios are shown in Fig. 8. As the shock wave moved through the driven section, the S value decreased due to that the distance L used in the scaling parameter S between the shock wave and contact surface became larger. S values at the pressure ratio of 10 are much higher due to higher Reynolds numbers than that at diaphragm pressure ratios of 20 and 100.

A smaller S value indicating that effects of the scale are more obvious on shock wave propagation demonstrates that much more attenuation happened in micro shock tubes. In the present case, lower S values were obtained at lower driven pressure. This indicates that S value also indicate effects of the low driven pressure in micro shock tubes.

Temperature contours of the flow in front of and after contact surface indicating the thickness of boundary layer are given in Fig. 9. A thicker boundary layer was obtained at diaphragm pressure ratio of 100 compared to that at diaphragm pressure ratios of 10 and 20. This results from the low pressure in the driven section for the case of high pressure ratio. This also indicates that the rarefaction caused by low pressure is more obvious in the case of low driven pressure in micro shock tubes. The boundary layer affects shock wave propagation with much more dissipation and viscous loss at lower driven pressure in micro shock tube. This makes the shock wave experience more attenuation. From contact surface locations, the contact surface at diaphragm pressure ratio of 100 propagated faster compared to that at diaphragm pressure ratios of 10 and 20. Based on Eq. (2), as the diaphragm pressure ratio increases, Mach number of the contact surface also increases.

The distributions of shock wave and contact surface velocity at different shock tube diameters are shown in Fig. 10. The distance L used to calculate the scaling pa-

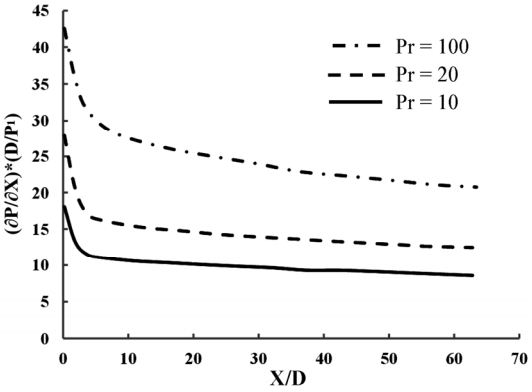

Fig. 6 Pressure gradient of the flow in front and after of shock wave for different cases (D=3mm)

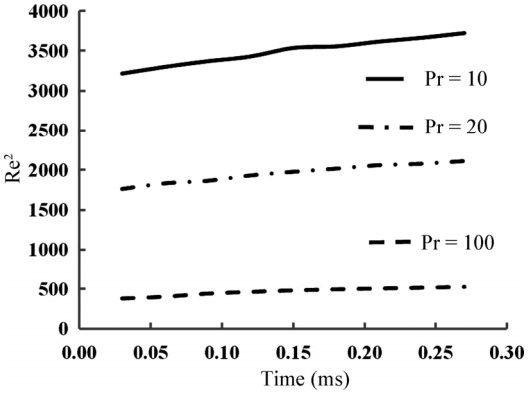

Fig. 7 Reynolds number distributions for different cases

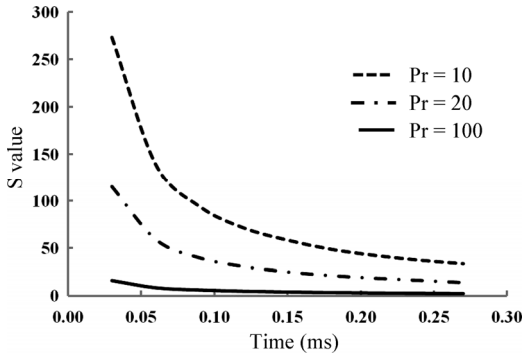

Fig. 8 S value distributions for different cases.

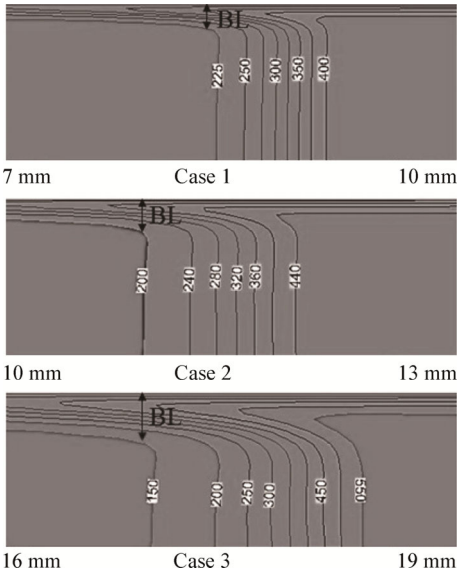

Fig. 9 Temperature contours for different cases at t=0.03ms

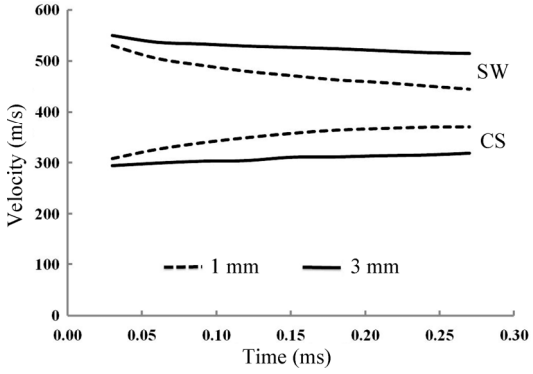

Fig. 10 Velocity distributions of shock wave and contact surface for different shock tube diameters.

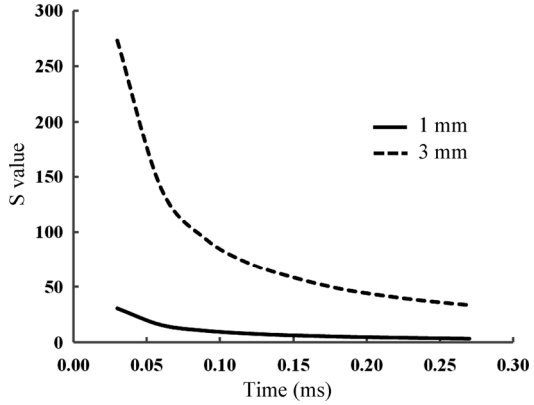

Fig. 11 S value distributions for different tube diameters

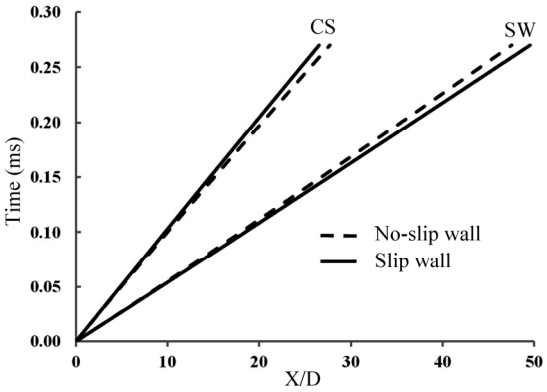

Fig. 12 Shock wave and contact surface locations for different wall boundary conditions

rameter S can be obtained. The shock wave velocity gradually decreased in both cases. This also indicates much stronger shock wave attenuation happened in the shock tube of smaller scale. The contact surface velocity gradually increased due to the boundary layer formation. Boundary layers near walls developed behind the shock wave, which makes the contact surface propagation similar to the contact surface moves through a nozzle that accelerates the contact surface. The shock wave velocity decreased faster at tube diameter of 1mm compared with that at tube diameter of 3mm, but the contact surface velocity increased in the shock tube of smaller diameter. This is mainly due to a thicker boundary layer developed behind the shock caused by effects of the scale in the shock tube of smaller diameter.

The distributions of scaling parameter S values at different shock tube diameters are shown in Fig. 11. As the shock wave moved in micro shock tube, the S value decreased due to that the distance L became larger. S values at the tube diameter of 3mm are much higher than that at the tube diameter of 1mm due to higher Reynolds numbers caused by larger diameter in the shock tube of 3mm diameter. From the theoretical Eq. (4), it is well known that as S value decreases, the effect of S value on calculating density ratios becomes more prominent. A smaller shock tube diameter and a lower pressure in driven section can make smaller S values that show expected effects of the scale.

Different wall boundary conditions were used to study the shock wave and contact surface propagation as is shown in Table 2. The locations of shock wave and contact surface are obtained as an x-t waves diagram in Fig. 12. SW represents shock wave, and CS is contact surface.

Shock wave at slip wall boundary condition propagated much faster than that at no slip boundary condition. This is due to the flow slipping near the wall for the slip case reduces friction effects between shock front and tube walls. In addition, the formation of boundary layer leads to much more attenuation at no slip boundary condition. The contact surface at no slip boundary condition propagated faster compared to that at slip wall boundary condition. This results from that a thicker boundary layer developed in the region between the shock wave and contact surface at the no slip case, which accelerated the contact surface.

The axis velocity contours at different wall boundary conditions are shown in Fig. 13. Case1 is for no slip wall case and case 5 is for the slip wall case. Obviously thick boundary layer developed behind the shock wave at no slip wall boundary condition, but this is no velocity jump in the radial direction at slip wall boundary condition. In the boundary layer, the velocity of the gas increases from zero near the wall to the maximum velocity of the flow. Based on shock wave locations, the shock wave propagated much faster at the slip case compared to that at no slip case. This is due to that there is an added velocity on the flow at slip case. In addition, another reason is that a turbulent boundary layer causes a larger momentum loss of the gas and leads to the rapid decay of the shock wave strength at no slip case.

Conclusions

Numerical simulations have been carried out to investtigate the propagation of shock wave and contact surface

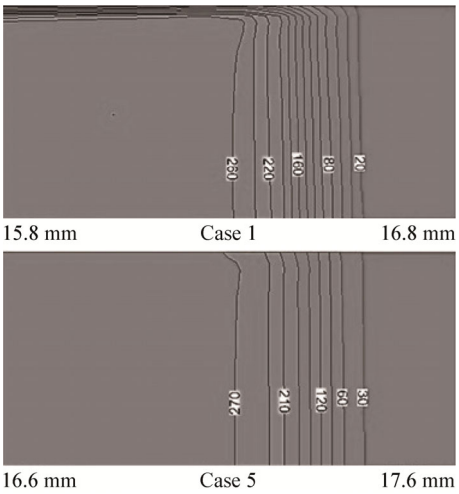

Fig. 13 Axial velocity contours for different wall boundary conditions at t=0.03 ms

boundary layer effects and effects of the scale were also studied. Results show that the initial diaphragm pressure ratio influences the shock wave and contact surface propagation. As the diaphragm pressure ratio increases, the shock wave strength and the contact surface propagation also increase. Shock wave gradually attenuates as it moves through the driven section, which results from the viscous effects, friction between shock front and tube walls and the boundary layer development in micro shock tubes. A thicker boundary layer that produces much more loss in flow momentum and shock wave propagation was also observed at a lower driven pressure in the micro shock tube. The pressure gradient of flow in front of and after shock wave increases as the diaphragm pressure ratio increases. The pressure gradient gradually decreases as shock wave moves in the shock tube due to the shock wave strength gradually decreases and the distance of pressure change across shock wave increases.

Much stronger attenuation resulting from viscous boundary layer formation and effects of the scale in shock wave propagation happens in the shock tube of smaller scale. Present results also show that the scaling parameter S can indicate effects of the micro scale and low pressure on shock wave propagation. The slip wall boundary condition was simulated by using Maxwell's slip condition. The utilization of slip wall boundary condition reduces the boundary layer effects and promotes shock wave propagation. In the future, an experimental study will be performed to validate the present theoretical conclusions and numerical results.

Acknowledgments

This work was supported by the National Research Foundation of Korea (NRF) grant funded by the Korea government (MEST) (2011-0017506).

References

[1] Duff. R. E., "Shock Tube Performance at Initial Low Pressure," *Phys. Fluids*, vol. 2, 1959, pp. 207–216.

[2] Brouillete. M., "Shock Waves at Microscales," *Shock Waves*, vol. 13, 2003, pp. 3–12.

[3] Mirels. H., "Test Time in Low Pressure Shock Tube," *Phys. Fluids*, vol. 6, 1963, pp. 1201–1214.

[4] Sturtevant. B. and Okamura. T. T., "Dependence of Shock Tube Boundary Layers on Shock Strength," *Phys. Fluids*, vol. 12, 1969, pp. 1723–1725.

[5] Kohsuke Tanaki, Kazuaki Inaba and Makoto Yamamoto, "Numerical Investigation on Transition of Shock Induced Boundary Layer," *47th AIAA Aerospace Science Meeting Including the New Horizons Forum and Aerospace Exposition*, January 2009, Orlando, Florida.

[6] Ngomo. D, Chaudhuri. A, Chinnayya. A. and Hadjadj. A., "Numerical Study of Shock Propagation and Attenuation in Narrow Tubes Including Friction and Heat Losses," *Computers & Fluids*, vol. 39, 2010, pp. 1711–1721.

[7] Sun. M., Ogawa. T. and Takayama. K., "Shock Propagation in Narrow Channels," *Proceedings of 24th Internationals Symposium on Shock Waves*, 2001, pp. 1321–1327.

[8] Xiao Hu, Toshiyuki Aoki and Naoya Tokura, "The Feature of Weak Shock Wave Propagated in an Overlong Tunnel," *Open Journal of Fluid Dynamics*, vol. 2, 2012, pp. 285–289.

[9] Bhasakaran. K. A. and Roth. P., "The Shock Tube as Wave Reactor for Kinetic Studies and Material Systems," *Progress in Energy and Combustion Science*, vol. 28, 2002, pp. 151–192.

[10] Zeitoun. D. E., Burtschell. Y. and Graur. I. A., "Numerical Simulation of Shock Wave Propagation in Micro Channels Using Continuum and Kinetic Approaches," *Shock Waves*, vol. 19, 2009, pp. 307–316.

[11] Zeitoun. D. E. and Burtschell. Y., "Navier-Stokes Computations in Micro Shock Tubes," *Shock Waves,* vol. 15, 2006, pp. 241–246.

[12] Arun. K. R. and Kim H. D., "Computational Study of the Unsteady Flow Characteristics of a Micro Shock Tube," *Journal of Mechanical Science and Technology*, vol. 27 (2), 2012, pp. 451–459.

[13] Arun K. R. and Kim H. D., "Numerical Visualization of the Unsteady Shock Wave Flow Field in Micro Shock Tube," *Journal of the Korean Society of Visualization*, vol. 10 (1), 2012, pp. 40–46.

[14] Park. J. O., Kim G. W. and Kim. H. D., "Experimental Study of the Shock Wave Dynamics in Micro Shock Tube," *Journal of the Korean Society of Propulsion Engineers*, vol. 17 (5), 2014, pp. 54–59.

[15] Karniadakis. G. E. M. and Beskok. A., "Micro Flows Fundamentals and Simulation," *Springer*, Berlin Heidelberg, New York, 2000.